Kinetic Studies of the Dry Reforming of Methane over the $Rh/La_2O_3-SiO_2$ Catalyst

John F. Múnera,[†] Laura M. Cornaglia,[†] Deborah Vargas Cesar,[‡] Martin Schmal,[‡] and Eduardo A. Lombardo*,[†]

Instituto de Investigaciones en Catálisis y Petroquímica (FIQ, UNL-CONICET), Santiago del Estero 2829, 3000 Santa Fe, Argentina, and NUCAT/PEQ/COPPE, Universidad Federal de Rio de Janeiro, C.P. 68052,21945-0, Rio de Janeiro, Brazil

$Rh(0.6\%)/La_2O_2(27\%)-SiO_2$ is one of the best catalysts used in membrane reactors for the CO_2 reforming of methane. A reliable rate equation is needed to model the system. Hence, the fresh and used catalysts were duly characterized using several instrumental techniques (TPD, DRIFTS, and XPS). The kinetic behavior of the catalysts in the reforming reaction was investigated as a function of temperature and partial pressure of CH_4 and CO_2. The rate of methane consumption showed fractional order dependency on the partial pressures of both reactants. A reaction mechanism adopted from the literature and supported by the characterization data presented here led to a kinetic equation that fits the experimental data obtained. This study contributes to a better qualitative and quantitative understanding of the dry reforming of methane occurring on Rh catalysts supported on La-containing oxides.

1. Introduction

The use of binary oxide systems as catalyst supports is very appealing because they combine the promotional catalytic effect of low surface area oxides such as La_2O_3 with high surface area solids such as Aerosil. Vidal et al.[1] have characterized this binary support exploring different $La_2O_3-SiO_2$ compositions and also $Rh/La_2O_3-SiO_2$ formulations after being used to catalyze both the hydrogenation of benzene and the hydrogenolisis of n-C_4H_{10} with good success.[2]

In a recent article, we reported the results obtained with $Rh/La_2O_3-SiO_2$ catalysts used in the dry reforming of methane.[3] These solids and particularly $Rh(0.6\%)/La_2O_3(27\%)-SiO_2$ had two valuable features: (i) They maintained the same surface area as the dry catalyst after calcination at 873 K. (ii) The dispersion of Rh^0 was much higher than that measured on calcined $Rh(0.6\%)/La_2O_3$. Moreover, and consistent with these features, the binary oxide supported Rh was more active than the Rh/La_2O_3 solid.[3]

The role of La_2O_3 as an active support in the Rh/La_2O_3[4] and Ni/La_2O_3[5] systems has been well documented. Essentially, lanthana helps to clean the catalyst surface by reacting the carbon formed during the reforming of methane with lanthanum oxycarbonates. These oxycarbonates are present in the bulk and at the surface of the solid, as shown by the Fourier transform infrared (FTIR) spectrum and the sharp C1s signal at ca. 289 eV, revealed by the X-ray photoeletron spectroscopy (XPS) data. As a matter of fact, this particular role of the active support is consistent with the fractional reaction order (0.38) with regard to CO_2 in the kinetic equation for the dry reforming of methane on Rh/La_2O_3.[4] Instead, when Rh and other noble metals are supported on noncarbonate forming oxides such as Al_2O_3, SiO_2, etc., the CO_2 order is zero as reported by Iglesia and co-workers.[6,7]

How does La_2O_3 interact in the binary solid? Bernal et al.[8] thoroughly characterized both $La_2O_3-Al_2O_3$ and $La_2O_3-SiO_2$ supports. In the former, they clearly detected the presence of an isolated La_2O_3 phase while, in the latter, only a low crystallinity mixed silicate phase was observed even for high La_2O_3 loadings. However, Bouarab et al.,[9] who characterized the $Co(5\%)/La_2O_3(50\%)-SiO_2$ system, were able to detect the characteristic reflection of La_2O_3 not seen by Vidal et al.[2] The key differences between these two studies are the different loadings and calcination temperatures.

Since nobody else has studied the dry reforming of methane on $Rh(0.6\%)/La_2O_3-SiO_2$, the only exception being our group, it is no wonder that no characterization data of this solid after reaction have been published. In an analogous fashion, no kinetic studies leading to the formulation of a reliable rate equation have been reported so far.

On the other hand, a number of valuable kinetic studies using other reforming catalysts have appeared[6,7,10,11] and they have been very useful in guiding our research. This essentially consisted of a thorough characterization of the catalyst to obtain hints along which to propose a reaction mechanism leading to a reliable kinetic equation. The reaction data were obtained using a micro-plug-flow reactor operated under differential conditions varying the reactants' partial pressures (2.5−40 kPa) and the reaction temperature (823−903 K). The temperature range was chosen to conform with the maximum of 873 K allowed by the requirements of the Pd−Ag alloy used in the membrane reactor in which this catalyst will be employed to produce pure hydrogen.

2. Experimental

2.1. Catalyst Preparation. The SiO_2 (Aerosil 300) employed in the preparation was previously calcined at 1173 K. The $La_2O_3(27\%)-SiO_2$ support was prepared by incipient wetness impregnation of SiO_2 with lanthanum nitrate (Anedra). The binary support was calcined at 873 K for 5 h. The metal deposition was performed with $RhCl_3 \cdot 3H_2O$ (Alfa) as a precursor compound. $Rh(0.6\%)/La_2O_3(27\%)-SiO_2$ was prepared by incipient wetness impregnation. The samples were kept at room temperature for 4 h and then dried overnight at 343 K. The catalyst was calcined in flowing air at 823 K

* To whom correspondence should be addressed. Tel/Fax: 54-342-4571162. E-mail: nfisico@fiqus.unl.edu.ar.

[†] Instituto de Investigaciones en Catálisis y Petroquímica (FIQ, UNL-CONICET).

[‡] Universidad Federal de Rio de Janeiro.

10.1021/ie061621p CCC: $37.00
Published on Web 04/05/2007 **PAGE EST: 6.7**

over 6 h and then was reduced in H_2 flow at 823 K for 2 h. The weight percents of Rh and La_2O_3 are shown in parentheses. A BET surface area of approximately 180 $m^2\ g^{-1}$ was measured for the $La_2O_3(27\%)-SiO_2$ catalyst and support.[3]

2.2. Kinetic Measurements. Kinetic studies under differential conditions were conducted in a conventional flow system consisting of a flow measuring and control system, a mixing chamber, and a fixed-bed reactor (5 mm i.d.), heated by an electric oven. The feed and product streams were analyzed with a thermal conductivity detector (TCD) gas chromatograph equipped with both a Porapak Q and a molecular sieve column. The mass of catalyst used was 10 mg; this was diluted with 50 mg of inert powder quartz to avoid temperature gradients. The effect of the feed flow rate and catalyst particle size of the $Rh/La_2O_3(27\%)-SiO_2$ catalyst on the reaction rate was experimentally determined. The measurements were conducted with a flow of 187 mL/min using catalyst particles in the 0.15−0.21 mm range. Conversions were usually controlled to be significantly lower than those defined by thermodynamic equilibrium (≤10%). Therefore, under the current reaction conditions, the reactor operates in the kinetic regime.

2.3. Catalyst Characterization. (A) Metal Dispersion. The Rh dispersion of the fresh catalyst, following the hydrogen reduction at 823 K for 2 h, was determined by static equilibrium adsorption of CO at room temperature in a conventional vacuum system, applying the double isotherm method.

(B) Temperature-Programmed Desorption (TPD) Experiments. These experiments were carried out using a setup which consists of a flow switching system, a heated reactor, and a quadrupole mass spectrometer (Prisma-Balzer). Approximately 200 mg of sample were loaded in the reactor.

Before the TPD analyses, all samples were purged under helium flow (50 mL min^{-1}) from room temperature up to 473 K at a heating rate of 10 K min^{-1}. The samples were then cooled to room temperature and reduced under flowing H_2 (30 mL min^{-1}) up to 823 K (5 K min^{-1}), then kept at this temperature for 2 h. After purging with He for 30 min, the sample was cooled under He flow. When the desired adsorption temperature was reached (773 K), the He flow was switched to CO_2. After 30 min, the sample was cooled to room temperature under CO_2 flow, and then, the lines were swept with He for 1 h. The temperature was increased at 10 K min^{-1} from 300 to 1173 K. The final temperature was kept constant for 1 h. The 44, 35, 28, and 18 mass numbers were monitored during the TPD experiments.

(C) In situ Diffuse Reflectance Fourier Transform Infrared Spectroscopy (DRIFTS). Experiments were carried out with a diffuse reflectance infrared cell (Spectra-Tech) with ZnSe windows, adapted to a FTIR Nicolet spectrometer (Nexus 470) with a mercury cadmium telluride (MCT) detector (4000−650 cm^{-1}).

In one set of experiments, the interaction of CO_2 with both the support and the catalyst was studied. In another case, the interaction of the same solid with the reaction mixture was monitored at varying temperatures. In all cases, the samples were loaded into the DRIFTS cell, then heated to 823 K under a flowing H_2/He mixture, and kept at this temperature for 2 h. In one experiment, the sample was cooled down to 423 K in flowing He; the solid was then exposed to a flowing stream of a 10% CO_2/He mixture to monitor the changes occurring in the IR spectra while increasing the temperature at a rate of 10 K min^{-1} up to 923 K. The spectra were taken at different

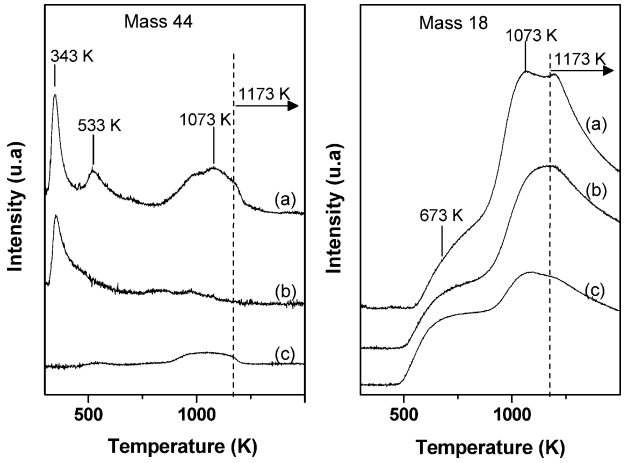

Figure 1. CO_2 TPD profiles tracked through the 44 and 18 amu signals of (a) reduced $Rh(0.6\%)/La_2O_3(27\%)-SiO_2$ treated in CO_2 at 773 K, (b) $La_2O_3(27\%)-SiO_2$ treated in CO_2 at 773 K, and (c) $Rh(0.6\%)/La_2O_3(27\%)-SiO_2$ without CO_2 treatment: heating rate 10 K min^{-1}.

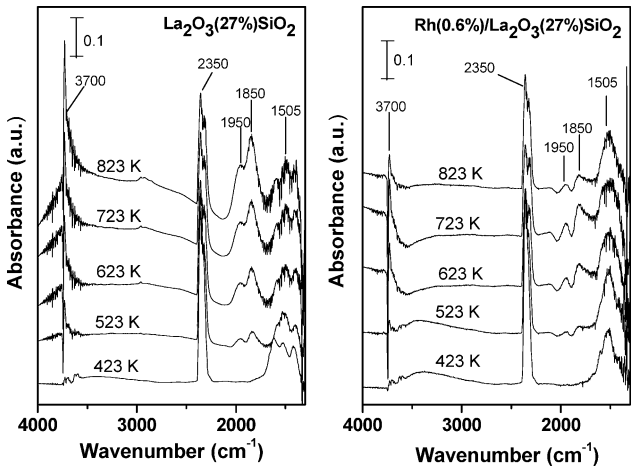

Figure 2. DRIFT spectra of $La_2O_3(27\%)-SiO_2$ and $Rh(0.6\%)/La_2O_3(27\%)-SiO_2$ during exposure to CO_2 at different temperatures, referenced to the spectrum of the reduced catalysts prior to gas admission.

temperatures. After each temperature was reached, it was kept constant for 10 min to stabilize the sample before taking the spectrum.

In an experiment designed to analyze the formation of species during the CO_2 reforming reaction, the samples were cooled down to 773 K in flowing He after reduction and then the reaction mixture was fed ($CH_4/CO_2/He = 1/1/18$). The reaction temperature was varied between 773 and 873 K. The spectrum of the sample after the reduction step was used as background.

(D) FT Infrared Spectroscopy (FTIR). The IR spectra were obtained using a Shimadzu FTIR 8101 M spectrometer with a spectral resolution of 4 cm^{-1}. The samples were prepared by compressing the pure solids at 2 tonnes cm^{-2} in order to obtain a self-supporting wafer (50 mg, 10 mm diameter). They were mounted in a transportable infrared cell with CaF_2 windows and external oven. The pretreatment was performed in a high vacuum system. The samples were first reduced at 723 K during 1 h in flowing H_2 and then outgassed for 1 h at 723 K in a dynamic vacuum of 7×10^{-4} Pa. After cooling to room temperature, a spectrum of the catalyst wafer was taken.

(E) X-ray Photoelectron Spectroscopy. The XPS measurements were carried out using a PHI model 1257 electron spectrometer. Non-monochromatic Al Kα X-ray radiation (1486.6 eV) was used. The photoelectron kinetic energy was measured with a hemispheric analyzer in 46.95 eV/step pass

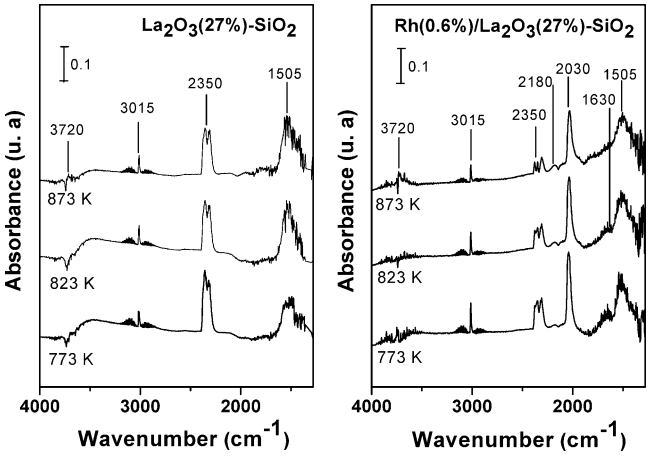

Figure 3. DRIFT spectra of $La_2O_3(27\%)-SiO_2$ and $Rh(0.6\%)/La_2O_3(27\%)-SiO_2$ during exposure to the reaction mixture $CO_2 + CH_4 + He$ (1:1:18) at different temperatures, referenced to the spectrum of the reduced catalysts prior to gas admission.

energy. The pressure in the analysis chamber was about 1×10^{-7} Pa during spectra collection.

The XPS spectra were recorded on the used catalyst and on the calcined solids, before and after treatment with hydrogen in the reaction chamber attached to the spectrometer. The samples were transferred to the analysis chamber without being exposed to air. The spectra of the La 3d, C 1s, Si 2s, O 1s, and Rh 3d core level regions were recorded for each sample.

3. Results

3.1. Characterization. 3.1.1. Temperature-Programmed Desorption Experiments. As a reactant, the CO_2 molecule was used to investigate the interaction of lanthana and silica in the mixed oxide support and in the catalyst. Figure 1 shows the TPD profiles for both of them after they were treated with flowing CO_2 at 773 K. The CO_2 traces ($m/e = 44$) of the reduced catalyst show two additional peaks at 533 and 1073 K besides the one appearing at 343 K for the support and the catalyst. The amount of desorbed CO_2 was determined from the TPD profiles. The μmol CO_2/μmol dispersed Rh ratio was equal to 3, suggesting that carbon dioxide interacts with the support. The water traces show $m/e = 18$ peaks at 673 and 1073 K. In no case were chlorine ($m/e = 35$) and CO ($m/e = 28$) detected in the TPD experiments.

3.1.2. In situ DRIFTS and FTIR Spectra. (A) CO_2 Adsorption. The DRIFTS spectra of the $La_2O_3(27\%)-SiO_2$ support and the Rh catalyst after reduction at 823 K and CO_2 adsorption as a function of temperature are shown in Figure 2. The sharp absorption band at 3700 cm^{-1} is most likely associated with the existence of isolated silanol groups.[12] The shoulder of this band at a lower wavenumber can be interpreted as being due to hydrogen bonded adjacent hydroxyls. The band at 2350 cm^{-1} corresponds to the gas-phase CO_2 contribution. It was observed that, at higher temperature, the band intensities at 1950, 1850, and 1630 cm^{-1} increased. These bands correspond to the vibrations of the silica skeleton (not shown). Note that well-defined bands at 1505 cm^{-1} of bicarbonate or carbonate species (Figure 2) and bands in the 3600−3700 cm^{-1} region (Figure 2) due to hydroxyl groups[12] already present on the support remain on the catalyst surface after CO_2 treatment at different temperatures.

(B) $CO_2 + CH_4$ Reaction. The DRIFTS spectra of the hydrogen treated support and the $Rh/La_2O_3(27\%)-SiO_2$ solid after exposure to the reacting mixture at 773−873 K are shown in Figure 3 including the gas-phase contributions of CO_2 (2350 cm^{-1}) and CH_4 (3015 cm^{-1}). On the catalyst, the bands at 2180 and 2030 cm^{-1} are assigned to CO (gas) and CO linearly adsorbed on Rh, respectively. No gem-dicarbonyls associated with a doublet at 2090−2100 and 2010−2034 cm^{-1} were observed. In a previous paper,[3] we studied the CO adsorption on this solid at temperatures lower than 473 K. We found that this species was transformed to Rh^0-CO (linear species) by a reductive agglomeration of highly dispersed Rh^0 at high temperature. A band at 1505 cm^{-1} characteristic of carbonate type species was detected on both solids. The formation of these species is favored when the reaction temperature is increased.[13] Note that the methane vibration intensity ($\gamma_{C-H} = 3015$ cm^{-1}) in the gas phase remained constant for the support, whereas the intensity in the catalyst spectra decreased due to the $CH_4 + CO_2$ reaction occurring at $T > 773$ K.

Importantly, no infrared CH bands have been detected in the 2700−2800 cm^{-1} region, corresponding to CH_x adsorbed species. This must be kept in mind when deciding about alternative reaction pathways (vide infra).

Table 1. Binding Energies[a] and Surface Concentration for $Rh(0.6\%)/La_2O_3(27\%)-SiO_2$

solid	$Rh3d_{5/2}$ (eV)	O1s (eV)	Rh[c]	La	O	Si
calcined at 823K	308.8 (3.4)[b]	531.6	1.5	12.2	72.4	13.8
	306.4 (3.1)					
H_2, in situ at 723 K	307.6 (3.8)	530.1	1.2	13.8	71.0	13.9
used at 823 K	307.1 (3.8)	531.8	1.6	6.5	76.6	15.2

[a] Contamination carbon was taken as reference at 284.4 eV. [b] The fwhm values are given between parentheses. [c] Percent values.

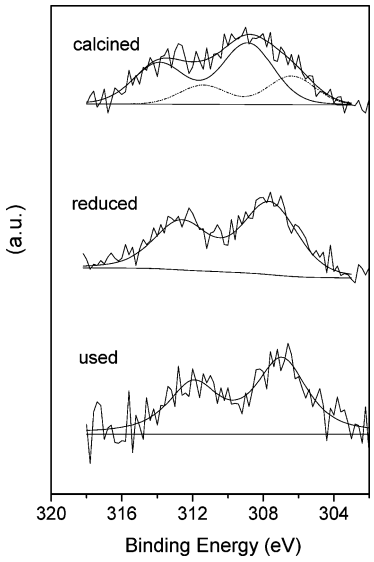

Figure 4. Rh3d XP spectra of $Rh(0.6\%)/La_2O_3(27\%)-SiO_2$ solid: calcined, after hydrogen reduction, and used in a fixed-bed reactor.

3.1.3. XPS Data. The XPS intensity ratios and binding energies (BEs) for $Rh(0.6\%)/La_2O_3(27\%)-SiO_2$ after calcination, in situ reduction at 723 K, and the CO_2 reforming of methane at 823 K are given in Table 1. Binding energies were referenced to C1s = 284.6 eV.

For the calcined solid, the Rh3d peak presents a full width at half-maximum (fwhm) = 4.8 eV (Figure 4), suggesting a mixture of Rh oxidation states. Two species were determined by the peak curve fitting; one appears at 308.8 eV and the other at 306.4 eV. According to the literature, a high-energy value indicates the presence of Rh^{n+} species. Values in the 307.6−309.6 eV range for Rh^+ compounds have been compiled by Nefedov et al.[14] However, other authors[15] have reported BEs

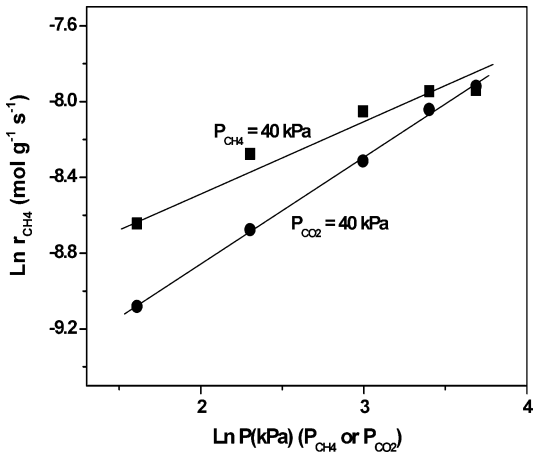

Figure 5. Order plots obtained using methane forward rates measured at 823 K.

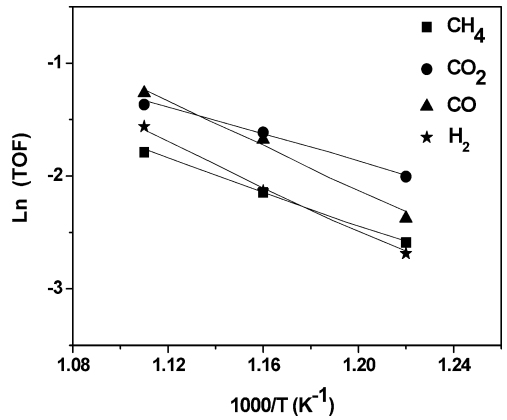

Figure 6. Arrhenius plots of reaction rates on Rh(0.6%)/La_2O_3(27%)−SiO_2: (reaction conditions) total pressure = 100 kPa, CO_2:CH_4:He = 1:1:1.

for Rh^{2+} compounds within a similar range (308.4−309.3 eV). The Rh^{3+} oxidation state presents a binding energy of 309.7 eV.[16] In the case of pure Rh metal foil, a Rh $3d_{5/2}$ peak occurs at 307.0 eV, with a 1.6 eV fwhm.[17]

The reduced catalyst shows a line width and a binding energy lower than those of the calcined sample, indicating reduction to Rh^0. The fwhm of the Rh $3d_{5/2}$ peak mainly reflects the particle size.[18−20] The increased fwhm for small particles, where the BE is also sensitively size dependent, originates from the particle size distribution. In the case of the reduced Rh(0.6)/La_2O_3 catalyst,[4] the binding energy was similar (307.0 eV); however, the fwhm was 1.8 eV. The reduced (fresh) and the used Rh(0.6%)/La_2O_3(27%)−SiO_2 catalyst show the same fwhm (3.7 eV). This indicates a similar average particle size in both samples. In agreement, for the reduced catalyst, the surface atomic concentration slightly decreases compared to that of the calcined and used samples, suggesting that no significant change in the rhodium dispersion has occurred. This is consistent with the high catalytic stability of this catalyst.[3]

The C 1s spectra only show one well-defined peak at 284.4 eV. No peak at 289.1 ± 0.2 eV, attributed to carbonate carbon,[18] is observed.

3.2. Kinetic Measurements. The reaction rates calculated from data obtained under differential conditions (CH_4 conversions ≤ 10%), varying the partial pressure of one reactant while maintaining the other constant, are plotted in Figure 5. From the slope of the two straight lines, the reaction orders for both

Table 2. Apparent Activation Energies for Reactants and Products[a]

	activation energies[b] E_{ap} (kcal mol^{-1})				
catalyst	r_{CH4}	r_{CO2}	r_{CO}	r_{H2}	ref
Rh(0.6%)/La_2O_3(27%)−SiO_2	14.7	11.8	20.5	20.7	this work
Rh(0.6%)/La_2O_3	12.7	13.0	14.2	18.9	4
Rh(3.8%)/SiO_2	19.0	21.7	20.8	23.4	21
Rh (1.0%)/MgO			20.0	23.0	22
Rh (1.0%)/TiO_2			12.0	16.0	22
Rh(1.0%)/Al_2O_3			16.0	18.0	22

[a] $CH_4 + CO_2 \leftrightarrow 2CO + 2H_2$. [b] Calculated from the following plot: ln(TOF) vs T^{-1}.

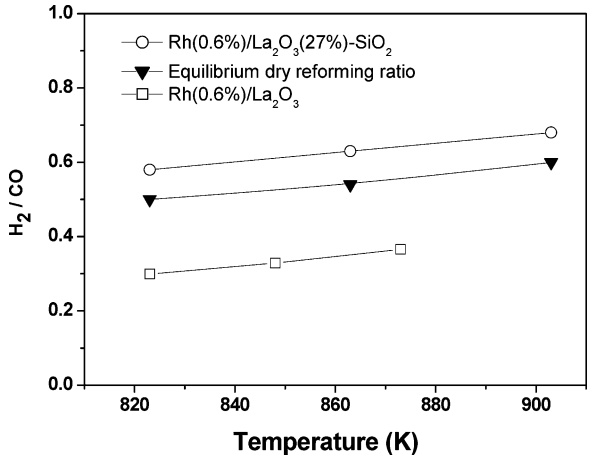

Figure 7. H_2/CO product ratio compared to the theoretical equilibrium ratio as a function of temperature: (reaction conditions) total pressure = 100 kPa, CO_2:CH_4:He = 1:1:1.

reactants are calculated and shown in the power law rate equation (eq 1).

$$r_{F(CH_4)} = k(P_{CH_4})^{0.56}(P_{CO_2})^{0.38} \quad (1)$$

Note that $r_{F(CH4)}$ is the forward rate of reaction calculated from the net rate of reaction (r_n) by

$$r_F = r_n(1 - \eta) \quad (2)$$

$$\eta = \frac{(P_{CO})^2(P_{H_2})^2}{(P_{CH_4})(P_{CO_2})}\frac{1}{K_e} \quad (3)$$

where P_i represents the prevalent pressures of reactants and products and K_e is the equilibrium constant calculated at the corresponding reaction temperature. Values of η range from 0.007 to 0.02 for the data reported here, lending additional reliability to the quality of the differential results.

3.2.1. Apparent Activation Energies. In order to compare our data with other results published in the literature, the apparent activation energies were calculated from Arrhenius-type plots for the turnover frequency (TOF) values of reactants and products (Figure 6), calculated from CO chemisorption data (Rh dispersion = 79%). The activation energies calculated from the slopes of these plots are collected in Table 2 and compared with similar data reported in the literature calculated in a similar partial pressure range. In our case, the activation energies for the disappearance of CH_4 and CO_2 are lower than those reported in the literature.[21,22] The activation energies for the formation of H_2 and CO are the same within the experimental error. Note that in all the other cases, the CO activation energy is 3−7 kcal

Table 3. Kinetic Model Parameters

parameters	temperatures		
	823 K	863 K	903 K
K_1[a,b]	$(48 \pm 4.27) \times 10^{-3}$	$(38 \pm 4.34) \times 10^{-3}$	$(30 \pm 3.18) \times 10^{-3}$
k_2[a,c]	$(6.0 \pm 0.48) \times 10^{-4}$	$(9.9 \pm 1.37) \times 10^{-4}$	$(1.9 \pm 0.31) \times 10^{-3}$
K_3k_4[a,d]	$(7.3 \pm 0.38) \times 10^{-5}$	$(8.7 \pm 0.33) \times 10^{-5}$	$(7.5 \pm 0.66) \times 10^{-5}$
K_3[a,e]	10.02 ± 0.110	3.74 ± 0.017	1.85 ± 0.003
k_4[f]	$(7.28 \pm 0.073) \times 10^{-6}$	$(2.32 \pm 0.0043) \times 10^{-5}$	$(4.05 \pm 0.0025) \times 10^{-5}$

[a] Values are reported at a ±95% confidence interval (data points = 6 for each linear regression). [b] Equilibrium constant of methane adsorption [kPa^{-1}]. [c] Rate constant of the decomposition of methane [mol g^{-1} s^{-1}]. [d] Product of the equilibrium constant of the reaction between CO_2 and La_2O_3 and the rate constant of reaction between the oxycarbonate species and carbon deposited on the surface of Rh [mol g^{-1} s^{-1} kPa^{-1}]. [e] From Shirsat et al.[24] [kPa^{-1}]. [f] Rate constant of the reaction between the oxycarbonate species and carbon formed on the surface of Rh [mol g^{-1} s^{-1}].

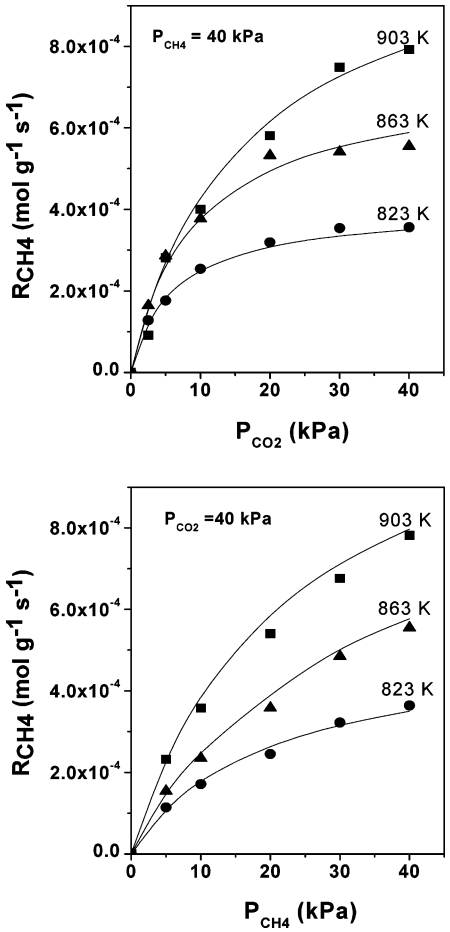

Figure 8. Fit of the proposed kinetic model for the CO_2 reforming of methane.

mol^{-1} lower than the H_2 activation energy. The evolution of the H_2/CO ratio with temperature parallels the curve obtained using the calculated equilibrium ratio (Figure 7). The latter ratio was calculated using the thermodynamic data for both the dry reforming and the RWGS. The H_2/CO ratio is much lower than unity, the value expected from the $CO_2 + CH_4$ stoichiometry, for both catalysts. The higher values obtained for Rh(0.6%)/La_2O_3(27%)−SiO_2 compared to those of Rh(0.6%)/La_2O_3 are consistent with the similar H_2 and CO activation energies determined for the former solid.

4. Discussion

4.1. The Presence of Oxycarbonates in the Reacting Catalyst. In our previous study of Rh/La_2O_3, we detected the presence of oxycarbonates on the surface and in the bulk of the catalyst.[4] The reaction mechanism involved the formation and decomposition of these compounds at the surface level. The similar reaction orders found in this system (eq 1) and with Rh/La_2O_3 are symptomatic of mechanistic similarities between these two solids. However, in the binary oxide support and catalyst, the oxycarbonates seem to be much less abundant than on La_2O_3.

The TPD of CO_2 from the catalyst (Figure 1, trace a) shows a wide peak centered at 1073 K that could be assigned to carbonates. In fact, Irusta et al.[23] studied the adsorption of CO_2 on Rh/La_2O_3 and found a desorption peak at 1070 K which was identified as corresponding to the decomposition of type II oxycarbonate. In the TPD data reported by Vidal et al.,[1] a similar, broad band centered at ca. 1050 K is clearly seen. However, the authors do not comment about this feature of their TPD profile. In our La_2O_3(27%)−SiO_2 solid, the XRD pattern exhibits broad reflections centered at $2\theta = 28°$ and 45°, which correspond to lanthanum disilicate. This may indicate that the availability of La_2O_3 to form the oxycarbonates is limited, and this probably means that they are formed at the surface level in minimum amounts. The released CO_2 detected in the TPD profile of the Rh catalyst corresponds to 2% of the total La_2O_3 present. The DRIFTS band observed at 1505 cm^{-1}, particularly on the catalyst (Figure 2), further supports the presence of some sort of carbonate (and/or bicarbonate) species. In the case of the binary support, no CO_2 desorption was observed at high temperature. This different behavior may suggest that Rh catalyzes the oxycarbonate formation in an oxidizing atmosphere.

4.2. Reaction Mechanism. Although there are quite a number of studies concerning the dry reforming of methane using metal/oxide catalysts, few of them concern the reaction mechanism and even less address the kinetic laws that govern their behavior. The more directly connected studies are those where La_2O_3 is used as a support, the reason being the significant difference in CO_2 adsorption between La_2O_3-supported catalysts and those built on top of Al_2O_3, SiO_2, ZrO_2, etc. As a matter of fact, in a very thorough series of papers, Iglesia and co-workers[6,7] showed that $r_{CH4} = kP_{CH4}$, which means that it is zero order with respect to CO_2. This is not the case for Ni/La_2O_3[5] and Rh/La_2O_3.[4] In these cases, the CO_2 reaction order varies between 0.37 and 0.50. This is symptomatic of the strong interaction between CO_2 and La_2O_3 which is reflected in the formation of oxycarbonates that were detected on these catalysts both at the surface and the bulk level at least after being exposed to the reacting mixture at $T \geq 823$ K.

In the case of Rh(0.6%)/La_2O_3(27%)−SiO_2, the proportion of oxycarbonate formed is much lower mainly due to the strong interaction between the oxides that restrict the La_2O_3 available to react with CO_2 possibly only at the surface level. From the results shown here, the two pieces of information that support the presence of the oxycarbonates are the TPD data (Figure 1) and the DRIFTS bands at 1505 cm^{-1} (Figure 2).

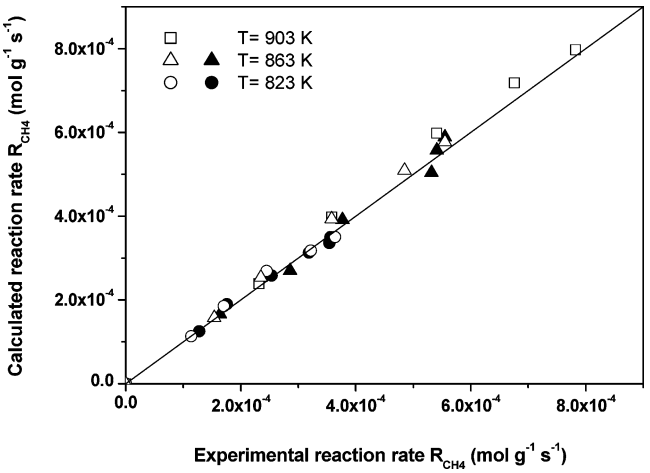

Figure 9. Parity plot. The data was obtained maintaining either P_{CO2} (full symbols) or P_{CH4} (empty symbols) constant.

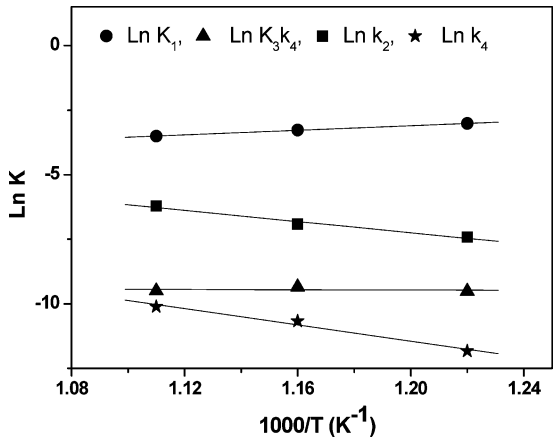

Figure 10. Arrhenius plots of the rate equation parameters.

In view of the above and the coincidence of the CO_2 reaction order in this system and in Rh(0.6)/La_2O_3, we propose for this system the same reaction mechanism already proved for Rh/La_2O_3 which in turn is based upon the mechanism proposed by Verykios et al.[5] for Ni/La_2O_3.

$$CH_4 + S \overset{K_1}{\longleftrightarrow} S{-}CH_4 \quad \text{equilibrium} \tag{4}$$

$$S{-}CH_4 \xrightarrow{k_2} S{-}C + 2H_2 \quad \text{slow step} \tag{5}$$

$$CO_2 + La_2O_3 \xrightarrow{K_3} La_2O_2CO_3 \quad \text{equilibrium} \tag{6}$$

$$La_2O_2CO_3 + C{-}S \xrightarrow{k_4} La_2O_3 + 2CO + S \quad \text{slow step} \tag{7}$$

In previous studies,[22] it has been shown that the CH_4 decomposition occurs on the metallic center and the CO_2 reaction on the support. This is reflected in the two pairs of reactions above, where eqs 4 and 5 are likely to represent the CH_4 decomposition on metal sites (S), eq 6 represents the chemical interaction between CO_2 and the support, and the slow reaction (eq 7) represents the "cleaning" operation that yields durable catalysts that do not deactivate by carbon accumulation. As a matter of fact, no carbon formation was detected in catalysts which were on stream for over 100 h using thermogravimetric analysis (TGA) and Raman spectroscopy, the latter being a highly sensitive tool to detect carbon present on solid oxides. The undetectability of carbon on Rh/La_2O_3(27%)−SiO_2 can be explained on the basis of the higher dispersion of Rh and La_2O_3 that should favor the cleaning slow step (eq 7) most likely occurring at the metal/support interface. Accordingly, the kinetic constant for the oxidation of the carbon species (Table 3), is greater than the equivalent rate constant measured for Rh/La_2O_3.

It could be argued that step 5 could be substituted by a series of H-abstraction steps. However, there is no experimental evidence that may support this option in our case, i.e., no C−H vibrations in the 2700−2800 cm^{-1} range are even hinted in the DRIFTS spectra obtained during $CH_4 + CO_2$ reaction (Figure 3).

4.3. Kinetic Modeling. The following rate equation (eq 8) that fits our data (Figure 8) was derived assuming that eqs 5 and 7 represent the slow steps and that the surface coverages of H_2 and CO adsorbed are negligible.

$$r_{CH4} = \frac{K_1 k_2 K_3 k_4 [CH_4][CO_2]}{K_1 K_3 k_4 [CH_4][CO_2] + K_1 k_2 [CH_4] + K_3 k_4 [CO_2]} \tag{8}$$

The effective rate constant values summarized in Table 3 were calculated from the linear plots $1/r$ vs $1/P_i$ (i = CO_2 or CH_4) keeping the other reactant pressure constant at each temperature. The parity plot (Figure 9) shows a very good correlation between the calculated and experimental reaction rates obtained at different temperatures.

Note that our model allows the calculation of both K_1, k_2, and the K_3k_4 product. In order to decouple this product, the thermodynamic data for calculating the K_3 values were obtained from Shirsat et al.,[24] as indicated in Table 3. The temperature dependence of k_i and K_i are shown in Figure 10 and reflected in the following equations (eq 9−12).

$$K_1 = 1.94 \times 10^{-4} \exp(4550/T) \quad [\text{kPa}^{-1}] \tag{9}$$

$$k_2 = 419.4 \exp(-11111/T) \quad [\text{mol g}^{-1}\,\text{s}^{-1}] \tag{10}$$

$$k_3K_4 = 1.023 \times \exp(-231.6/T) \quad [\text{mol g}^{-1}\,\text{s}^{-1}\,\text{kPa}^{-1}] \tag{11}$$

$$k_4 = 2091 \exp(-15955/T) \quad [\text{mol g}^{-1}\,\text{s}^{-1}] \tag{12}$$

Note that both the methane adsorption enthalpy and entropy are negative, in this way lending additional credibility to the mechanistic model and the assumptions made in deriving the kinetic equation (eq 8).

The methane adsorption enthalpy is −9.0 kcal/mol. For the adsorption of CH_4 on metal surfaces, it has been reported[25] that the adsorption energies involved are small, with magnitudes lower than 0.2 eV (4.5 kcal/mol). The similarity of those two values also supports our proposed mechanism.

5. Conclusions

- A reaction mechanism involving the chemical interaction between CO_2 and the support, similar to the one proposed for Ni/La_2O_3[5] and Rh/La_2O_3[4] catalysts, has been considered.
- The binary support contains lanthanum disilicate. However, small amounts of lanthanum carbonates are revealed by the CO_2 TPD and DRIFTS data on the binary support and Rh catalyst. It has been estimated that ca. 2% of the La_2O_3 load could be available to form carbonates in the presence of CO_2.
- The rate equation derived from the model neatly fits the experimental data obtained between 823 and 903 K (Figure 8),

and the parity plot (Figure 9) confirms this observation. Furthermore, both the methane adsorption entropy and enthalpy are negative (eq 10), lending additional support to the proposed model.

- Rh anchored to the binary support is better dispersed than on La_2O_3 (79% vs 14% dispersion), and the surface area of the former is much higher than that of the single oxide. It has been previously shown that the stability of both systems is identical.[3]
- The k_2 rate constant expressed by the metal sites shows similar values for both solids ($k_2 = 12.96\ s^{-1}$). However, k_4 is lower when Rh is supported on La_2O_3 (27%)$-SiO_2$ than on pure La_2O_3, i.e., at 823 K, $k_4 = 0.16$, and $0.36\ s^{-1}$ for the binary support and pure La_2O_3, respectively.

Acknowledgment

The authors wish to acknowledge the financial support received from UNL, CONICET, ANPCyT, and CNPq. They are also grateful to Elsa Grimaldi for the English language editing.

Literature Cited

(1) Vidal, H.; Bernal, S.; Baker, R. T.; Finol, D.; Pérez Omil, J. A.; Pintado, J. M.; Rodríguez-Izquierdo, J. M. Characterization of La_2O_3/SiO_2 Mixed Oxide Catalyst Supports. *J. Catal.* **1999**, *183*, 53.

(2) Vidal, H.; Bernal, S.; Baker, R. T.; Cifredo, G. A.; Finol, D.; Rodríguez-Izquierdo, J. M. Catalytic Behavior of Lanthana-promoted Rh/SiO_2 Catalysts: Influence of the Preparation Procedure. *Appl. Catal. A: Gen.* **2001**, *208*, 111.

(3) Irusta, S.; Múnera, J.; Carrara, C.; Lombardo, E. A.; Cornaglia, L. M. A Stable, Novel Catalyst Improves Hydrogen Production in a Membrane Reactor. *Appl. Catal. A: Gen.* **2005**, *287*, 147.

(4) Múnera, J. F.; Irusta, S.; Cornaglia, L. M.; Lombardo, E. A.; Vargas, C. D.; Schmal, M. Kinetics and Reaction Pathway of the CO_2 Reforming of Methane on Rh Supported on Lanthanum-based Solids. *J. Catal.* **2006**, *245*, 25.

(5) Verykios, X. E. Catalytic Dry Reforming of Natural Gas for the Production of Chemicals and Hydrogen. *Int. J. Hydrogen Energy* **2003**, *28*, 1045.

(6) Wei, J.; Iglesia, E. Structural Requirements and Reaction Pathways in Methane Activation and Chemical Conversion Catalyzed by Rhodium. *J. Catal.* **2004**, *225*, 116.

(7) Wei, J.; Iglesia, E. Reaction Pathways and Site Requirements for the Activation and Chemical Conversion of Methane on Ru-Based Catalysts. *J. Phys. Chem. B* **2004**, *108*, 7253.

(8) Bernal, S.; Blanco, G.; Calvino, J. J.; Cauqui, M. A.; Rodríguez-Izquierdo, J. M.; Vidal, H. Influence of the Preparation Procedure on the Chemical and Microstructural Properties of Lanthana-promoted Rh/SiO_2 Catalysts. A FTIR Spectroscopic Study of Chemisorbed CO. *J. Alloys Compd.* **1997**, *250*, 461.

(9) Bouarab, R.; Cherifi, O.; Auroux, A. Effect of the Basicity Created by La_2O_3 Addition on the Catalytic Properties of Co(O)/SiO_2 in $CH_4 + CO_2$ Reaction. *Thermochim. Acta* **2005**, *434*, 69.

(10) Souza, M. M.; Aranda, D. A.; Schmal, M. Reforming of Methane with Carbon Dioxide over $Pt/ZrO_2/Al_2O_3$ Catalysts. *J. Catal.* **2001**, *204*, 498.

(11) Bradford, M. C. J.; Vannice, M. A. CO_2 Reforming of CH_4 over Supported Pt Catalysts. *J. Catal.* **1998**, *173*, 157.

(12) Blanco, G.; Calvino, M. A.; Cauqui, M. A.; Cifredo, G. A.; Pérez, J. A. Characterization of Silica Dispersed Lanthana by CO_2 Adsorption. *J. Alloys Compd.* **1994**, *207*, 201.

(13) Ferreira, A. P.; Rodríguez, R. I.; Anderson, J. A.; Guerrero, R. A. Mechanistic Aspects of the Dry Reforming of Methane over Ruthenium Catalysts. *Appl. Catal. A: Gen.* **2000**, *202*, 183.

(14) Nefedov, V. I.; Firsov, M. N.; Shaplygin, I. S. Electronic Structures of $MRhO_2$, MRh_2O_4, $RhMO_4$ and Rh_2MO_6 on the Basis of X-ray Spectroscopy and ESCA Data. *J. Electron Spectrosc. Relat. Phenom.* **1982**, *26*, 65.

(15) Gysling, H. J.; Monnier, J. R.; Apai, G. Synthesis, Characterization, and Catalytic Activity of $LaRhO_3$. *J. Catal.* **1987**, *103*, 407.

(16) Polychronopoulou, K.; Fierro, J. L.; Efstathiou, A. M. The Phenol Steam Reforming Reaction over MgO-based Supported Rh Catalysts. *J. Catal.* **2004**, *228*, 417.

(17) Kawai, M.; Uda, M.; Ichikawa, M. The Electronic State of Supported Rhodium Catalysts and the Selectivity for the Hydrogenation of Carbon Monoxide. *J. Phys. Chem.* **1985**, *89*, 1654.

(18) Gallaher, G. R.; Goodwin, J. G.; Huang, Ch. Sh.; Houalla, M. XPS and Reaction Investigation of Alcali Promotion of Rh/La_2O_3. *J. Catal.* **1993**, *140*, 453.

(19) Zafeiratos, S.; Nehasil, V.; Ladas, S. X-ray Photoelectron Spectroscopy Study of Rhodium Particle Growth on Different Alumina Surfaces. *Surf. Sci.* **1999**, *433*, 612.

(20) Labich, S.; Taglauer, E.; Knozinger, H. Metal-support Interactions on Rhodium Model Catalysts. *Top. Catal.* **2001**, *14*, 153.

(21) Sigl, M.; Bradford, M. C. J.; Knozinger, H.; Vannice, M. A. CO_2 Reforming of Methane over Vanadia-promoted Rh/SiO_2 Catalysts. *Top. Catal.* **1999**, *8*, 211.

(22) Erdohelyi, A.; Cserenyi, J.; Solymosi, F. Activation of CH_4 and its Reaction with CO_2 over Supported Rh Catalysts. *J. Catal.* **1993**, *141*, 287.

(23) Irusta, S.; Cornaglia, L. M.; Lombardo, E. A. Effects of Rhodium and Platinum on the Reactivity of Lanthanum Phases. *Mater. Chem. Phys.* **2004**, *86*, 440.

(24) Shirsat, A. N.; Ali, M.; Kaimal, K. N. G.; Bharadwaj, D. D. Thermochemistry of $La_2O_2CO_3$ Decomposition. *Thermochim. Acta* **2003**, *399*, 167.

(25) Chak, T. A.; Ching, F. N.; Meng, S. L. Methane Dissociation and Syngas Formation on Ru, Os, Rh, Ir, Pd, Pt, Cu, Ag, and Au: A Theoretical Study. *J. Catal.* **1999**, *185*, 12.

Received for review December 16, 2006
Revised manuscript received February 23, 2007
Accepted February 26, 2007

IE061621P